FINAL TECHNICAL REPORT FOR GRANT NUMBER: G11AP20196

LABORATORY EXPERIMENTS ON ROCK FRICTION FOCUSED ON UNDERSTANDING EARTHQUAKE MECHANICS

Terry E. Tullis
Tele: (401) 863-3829
FAX: (401) 863-2058
Email: Terry_Tullis@brown.edu

and

David L. Goldsby
Tele: (401) 863-1922
FAX: (401) 863-2058
Email: David_Goldsby@brown.edu

Both at

Brown University
Department of Geological Sciences
Providence RI 02912-1846

August 1, 2011 to July 31, 2012

ABSTRACT

In order to determine where best to deploy limited resources for mitigating earthquake loss in the US, we need to understand when and where earthquakes may occur and how intense their accelerations can be. Every time an earthquake occurs, we gain more understanding of the earthquake problem through measurements of ground motion and modeling of seismic sources. In addition to information derived from earthquakes, we also benefit from improved understanding of the seismic source through laboratory measurements and modeling, to anticipate phenomena that may occur in future earthquakes. One of the great gaps in our understanding of source processes is how shear resistance varies on a fault during rapid coseismic slip and what this implies about the magnitudes of stress drops and near-fault accelerations. We will help fill that gap through our proposed laboratory experiments.

During recent years we have conducted research to understand two potential dynamic fault-weakening mechanisms: flash heating and thermal pore-fluid pressurization. This year we have continued these efforts, but have focused exclusively on thermal pore-fluid pressurization. This focus was directed by the USGS review panel and it makes sense because we are in a unique position to study this process. This unique opportunity derives from the fact that our high-pressure rotary-shear apparatus is the only apparatus in existence that combines arbitrarily large slip displacement with independent control of both confining pressure and pore pressure. In other words, ours is the first study in which this mechanism is isolated and characterized under controlled conditions on confined samples (e.g., with fully saturated rocks of controlled fluid pressure and proscribed permeabilities of the rocks).

During the past year we have 1) developed a successful protocol for thermally cracking our initially low permeability Frederick diabase samples ($<10^{-23}$ m^2) and measuring the resulting permeabilities in the range 10^{-23} m^2 to 10^{-19} m^2 range, 2) conducted a suite of bare-surface and gouge experiments with samples of several different permeabilities, including one so low that 3 weeks was required to saturate the sample, 3) discovered that dilatancy in many situations tends to reduce the pore pressure enough that thermal pressurization does not overcome it, and 4) observed some weakening which appears to due to thermal pressurization. In addition, we have done extensive thermal modeling via a FEM model that demonstrates that the temperature rise in our experiments is sufficiently low that only modest thermal pressurization effects are expected. This understanding places us in an excellent position to conduct more definitive experiments going forward. In particular, by sliding at up to 16 mm/s at a confining pressure of 100 MPa, our modeling suggests that the temperature rise should be up to 600 ^{o}C, rather than the ~25 ^{o}C rise estimated for our current results. To minimize the fluid-pressurization-limiting effects of dilation, we believe that new experiments will prove to be useful in which 1) enough sliding is accrued that a trend of compaction is established, 2) the sliding velocity is then set to zero, 3) then enough time is allowed for the pore pressure to return to its externally applied value, and 4) then sliding is commenced at high velocity.

Constitutive equations for thermal pore-fluid pressurization are being employed in dynamic-rupture models, so it is imperative that we better understand the underlying physics of this mechanism. At present there are literally no other experimental data that bear conclusively on this mechanism. Through our continuing study of thermal pressurization of pore fluids, we seek to understand how the shear resistance on faults varies during earthquakes and what the observed behavior implies for earthquake rupture and strong ground motion.

INTRODUCTION

During the past years, we have been investigating the frictional properties of rocks at seismic slip rates. Our experiments to date reveal that two distinct weakening mechanisms occur at sliding velocities above ~1 mm/s. First, a previously unknown mechanism, silica-gel weakening, operates above velocities of ~1 mm/s and requires hundreds of mm of slip to be activated [*Di Toro et al.*, 2004; *Goldsby and Tullis*, 2002]. Second, flash weakening of asperity contacts operates above ~0.1 m/s (for many crustal silicate rocks) and requires only fractions of a mm of slip to be effective [*Beeler et al.*, 2008; *Goldsby and Tullis*, 2011; *Kohli et al.*, 2011; *Rice*, 2006].

Although further research investigating the details of these mechanisms and their applicability to earthquakes is warranted, we have turned our attention to the widely discussed mechanism of weakening due to thermal pressurization of pore fluids. In site of the fact that there are many theoretical and numerical studies of this weakening mechanism [*Andrews*, 2002; *Lachenbruch*, 1980; *Lee and Delaney*, 1987; *Mase and Smith*, 1985, 1987; *Noda*, 2008; *Noda and Shimamoto*, 2005; *Rempel and Rice*, 2006; *Rice*, 2006; *Rice and Cocco*, 2007; *Sibson*, 1973] and it is increasingly used in dynamic rupture and earthquake nucleation models [*Bizzarri and Cocco*, 2006a, b; *Lapusta and Rice*, 2004a, b; *Noda and Lapusta*, 2010; *Noda et al.*, 2009; *Rice et al.*, 2010; *Schmitt and Segall*, 2009; *Segall and Rice*, 2006], there are no experimental studies that conclusively demonstrate the operation of this process. Consequently it is important to determine if its occurrence can be demonstrated and its relevance for earthquakes can be evaluated. Below we describe our progress in conducting experiments on this difficult-to-study weakening mechanism.

The experiments are being conducted on fine-grained Fredrick diabase that we collected from its type location in Maryland [*Adams and Gibson*, 1929]. Diabase is used because it does not undergo gel weakening at large slip displacements and high slip rates as do other silicate rocks of higher silica content [*Roig Silva et al.*, 2004a, b], and does not weaken due to flash heating at the modest (sub-0.1 m/s) slip rates of our experiments [*Goldsby and Tullis*, 2011]. Thus any observed weakening due to thermal pore-fluid pressurization will not be convolved with that due to other known mechanisms. This expectation has been borne out by our experiments to date as detailed below. A further advantage of this rock is that in its original state its permeability is so low (less than 10^{-23} m/s^2 according to our measurements) that it impractical to saturate it in reasonable laboratory times. However, by subjecting the diabase to a thermal treatment to a variety of peak temperatures it is possible to create higher permeabilities, and in this way we have been able to control the permeability over the range from 10^{-23} to 10^{-18} m^2. Because the permeability is a critical parameter for thermal pressurization, this allows us to compare the experimental results with the theoretical predictions for the rate of weakening with slip as a function of both slip velocity and permeability.

Dynamic weakening due to thermal pressurization of pore fluids

Within the past year, we have made important progress in our investigation of the dynamic fault weakening mechanism termed thermal pore-fluid pressurization. A critical component of our experiments is the protocol we developed for systematically varying the permeability of Frederick diabase samples, one of the most critical parameters that determines whether pore fluids become pressurized during coseismic frictional heating. As we have detailed previously, we chose Frederick diabase for our thermal-pressurization experiments for two reasons – 1) because it does not weaken due to the development of a silica (or silicate) gel on the sliding surface, and 2) because thermal-cracking experiments have been previously conducted on this material by other workers, suggesting a means for varying the permeability of the samples via

heat treatment. Below we demonstrate how we varied the permeability of the samples via thermal cracking, and then detail our new high-speed friction experiments on these samples to investigate thermal pressurization.

Permeability variation with the degree of thermal cracking – Following previous experimental studies of thermal cracking of Frederick diabase [*Fredrich and Wong, 1986*], we introduced microcracks into a suite of diabase samples by subjecting them to a known temperature excursion prior to epoxying them (at room temperature) in our steel sample grips in preparation for testing. The samples become cracked during heating due to mismatches in the thermal expansion coefficient between neighboring grains (each grain is anisotropic in its thermal expansion coefficient), which can generate high-enough grain-scale stresses to fracture the samples along grain boundaries. If these grain boundary cracks are interconnected, they result in an increase in the permeability of the rock.

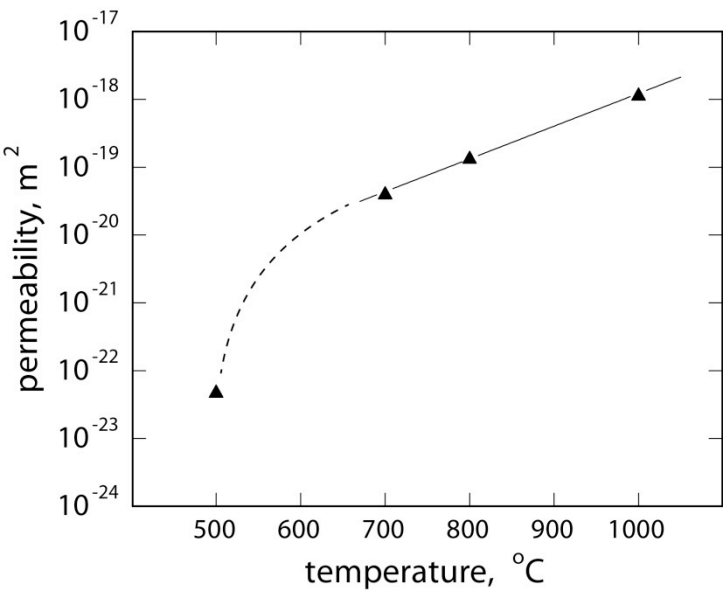

Figure 1 – Permeability of Frederick diabase samples as a function of maximum temperature of heat treatment. Data suggest a threshold for thermal cracking of ~600 °C.

We introduced cracks into our samples by heating them to temperatures of 500, 700, 800 and 1000 °C. After the samples were subsequently epoxied into the sample grips in preparation for testing, we then pressurized the samples in our high-pressure rotary-shear apparatus with our flow-through pore-pressure tubing installed in the sample assembly. By applying a constant pressure head to the lower sample ring, with the downstream pore-pressure port (in the upper sample grip) at atmospheric pressure, we were able to fully saturate even low-permeability samples (i.e., $<10^{-19}$ m^2). By measuring the volumetric flow rate through the sample and from the known cross-sectional area of the sample rings, we were able to determine the permeability of each sample (see below). A sample was deemed 'saturated' when bubble-free flow of water was observed through the pore pressure tubing connected to the upper sample grip. For the lower permeability samples, this saturation step took 1 to 3 weeks.

From the volumetric flow rate through the sample Q and the applied pressure gradient $\frac{\Delta P}{\Delta L}$, it is straightforward to calculate the permeability K of the samples via Darcy's law:

$$K = \frac{Q}{A}\mu\frac{\Delta L}{\Delta P}$$

where A is the cross-sectional area of the sample ring, and μ is the viscosity of water. In Figure 1, we plot the permeabilities calculated from the volumetric flow rate and the pressure gradient applied to each sample. As shown in Figure 1, the permeability varies systematically from a low

of 5×10^{-23} m^2 for the sample heated to 500 ^oC to 1×10^{-18} m^2 for the sample subjected to the 1000-^oC treatment. Based on theoretical predictions of thermal-pressurization behavior [e.g., *Mase and Smith*, 1987, see their Fig. 6], such permeabilities were expected to give rise to dramatic thermal pressurization effects even at the comparatively low sliding speeds and normal stresses of our experiments.

High-speed friction experiments on saturated samples – After saturating the samples as described above and measuring the permeability of the samples, the specimens were removed from the high-pressure apparatus and the lower flow-through pore-pressure tubing, which is incompatible with rotating the lower sample grip to the large sliding displacements required to observe thermal pressurization, was removed. The pore-pressure port in the lower sample grip was then plugged, and the sample was repressurized in the gas apparatus in preparation for testing, and fluid pressure was applied via pore-pressure tubing connected to the top stationary sample grip. In this manner, we could control (or at least attempt to control, see below) the pore pressure during large-displacement, high-speed frictional sliding.

Gouge experiments – All of the experiments but one were conducted on initially bare surfaces of Frederick diabase. One experiment, however (309pfp), was conducted on Frederick diabase gouge. This simulated gouge was prepared by mechanically crushing a sample of Frederick diabase in a ball mill, then using all powders that passed a 75-micron sieve as the specimen. The 1-mm thick gouge specimen was sandwiched between very permeable Fontainebleau sandstone forcing blocks during the experiment. The sample was saturated in its precompacted (unpressurized) state using a gravity feed of water on the laboratory bench. No attempt was made to measure the permeability of the sample during saturation. Once saturated, the pore-pressure port in the lower sample grip was plugged, and the sample was pressurized in the gas apparatus in preparation for sliding. During the experiment, fluid pressure was controlled (or an attempt was made to control fluid pressure) by applying constant pressure through the pore-pressure tubing connected to the upper sample grip.

Experimental results – Five experiments have been conducted on both room-dry and water-saturated samples with initially bare sliding surfaces with the permeabilities shown in Figure 1, and one experiment was conducted on saturated gouge. Figure 2 shows a summary plot of the experimental data from these six friction experiments. All of the summary plots except the one for Experiment 297fd show four experimental variables plotted against the sliding displacement – 1) shear stress, 2) fault-normal displacement (measured with an LVDT inside the pressure vessel, close to the sliding surface), 3) the position of the piston in the pore-fluid volumometer (which, plotted against time, gives the volumetric flow rate through the sample during the saturation step, and during sliding gives the change in position required to maintain a constant applied fluid pressure), and 4) the sliding velocity.

Three key observations from the experiments are that 1) dilation (a negative slope of fault-normal displacement with slip) was observed initially in the bare surface experiments to a remarkably consistent slip of ~0.5 m, followed by 2) compaction for the remainder of each test; 3) the friction coefficient, which is the measured shear stress divided by the assumed effective normal stress (equal to the normal stress minus the pore pressure applied at the top of the top sample), is much higher in some cases than the nominal friction coefficient of 0.8 (see upper left figure without pore fluid), indicating that the actual pore pressure in those tests is *less than* the applied fluid pressure. This discrepancy highlights the influence of dilation and low permeability

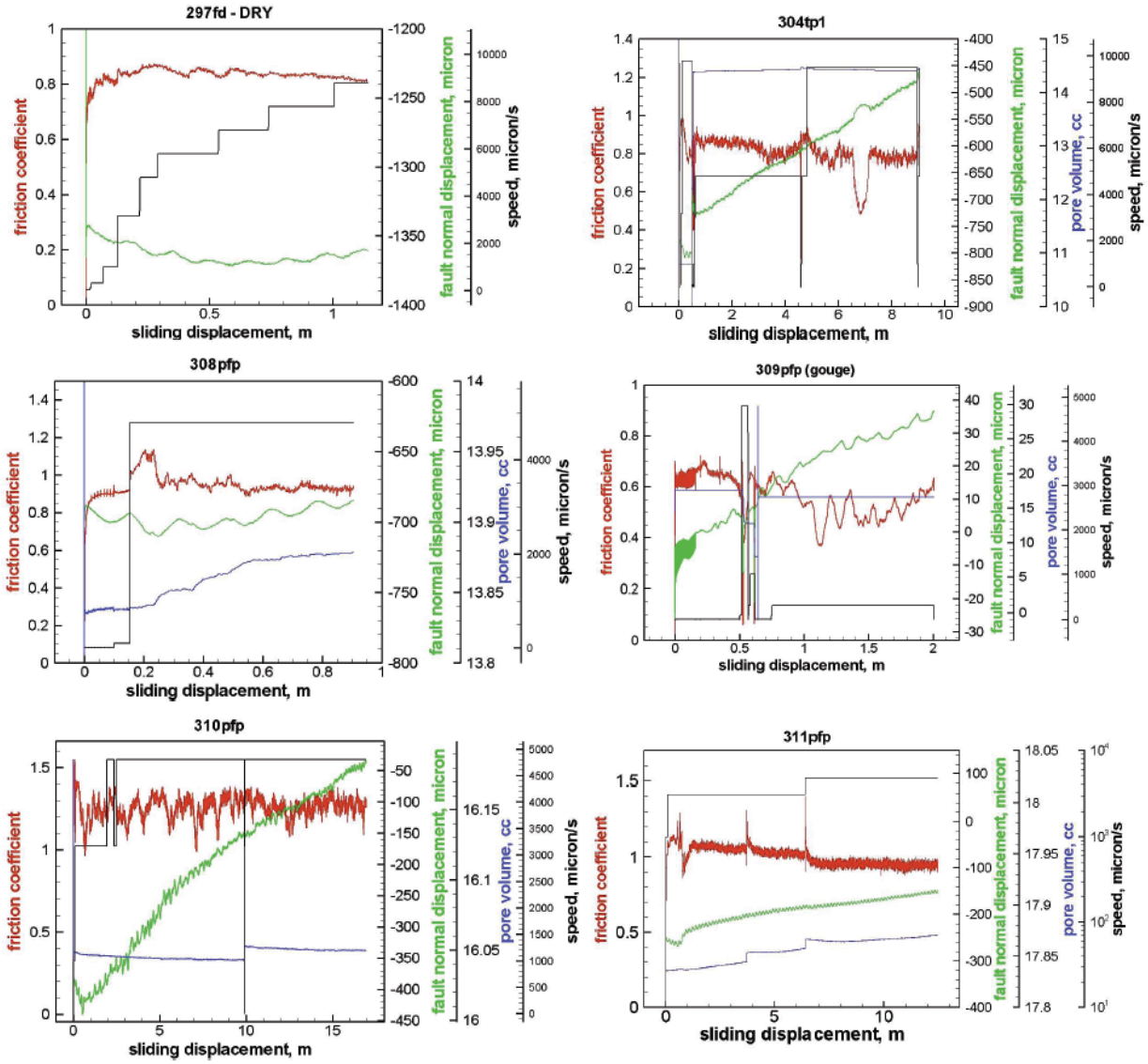

Figure 2 – Summary plots of the data from 5 runs on initially bare surfaces of Frederick diabase and data from one test on simulated gouge (309pfp). Several of the experiments were terminated by a leak of the confining pressure to the sample (resulting data are not shown; in 309pfp, two leaks to confining pressure were observed at each of the two steps to V=4.8 mm/s, however, atypically, those leaks healed and allowed the experiment to be completed. Note the dilation trends (negative slope of fault normal displacement with slip) in all but the gouge experiment over the first ~0.5 m of slip, followed by a compaction trend (positive slope of fault normal displacement vs. slip) in each case. Note very high friction in 308pfp, 310pfp and 311pfp, due to actual pore pressures being lower than those applied (see text for details).

on the pore pressure on the fault surface, and the difficulty of externally controlling fluid pressure for low-permeability samples. In the 311pfp plot, note the exponential-like decay in friction over a sliding displacement of ~0.5 m that occurs at sliding displacements of ~3 and ~7 m (see below for more details).

As shown in Figure 2, the friction coefficient in the dry case and the saturated, drained case (297fd and 304pfp, respectively) obtains values of 0.81 to 0.84. This level of friction is assumed to be the 'normal' friction coefficient for diabase in wet and dry (i.e., in an "as-is" state of dryness) conditions. For Experiments 308pfp, 310pfp, and 311pfp, however, the apparent

friction coefficient is ~1, 1.3, and 1.1, respectively, indicating that the pore pressure of the samples was less than the applied fluid pressure. These high values of friction were likely caused by dilation of the fault zone (see below), which lowered the fluid pressure. Because the rocks have such low permeabilities, and the constant applied fluid pressure can only communicate with the fault zone through the low-permeability sample rings, the fluid pressure within the fault zone takes a long time to equilibrate with the applied fluid pressure (much longer than the timescale of the sliding experiments). Thus, even small amounts of dilation can significantly decrease the fluid pressure, which cannot equilibrate with the applied pressure over the relatively short timescale of the experiment.

To estimate the real fluid pressure on the fault in each experiment, we assumed that the 'real' friction coefficient for Frederick diabase is 0.8, that the effective pressure law holds for our experiments, and that the fluid pressure could then be estimated by determining what the fluid pressure would have to be to yield a value of the friction coefficient of 0.8 given the observed shear stress and the applied normal stress. The results of this calculation are shown in Table 1:

Table 1 – Normal stress, applied fluid pressure, real fluid pressure in fault zone, difference between applied and real fluid pressures, and permeability for six thermal-pressurization experiments.

Experiment number	**Normal stress, MPa**	**Applied fluid pressure, MPa**	**Real fluid pressure, MPa**	**Applied P – real P**	**Permeability, m^2**
297fd	25	0	0	0	$\leq 5.0 \times 10^{-23}$
304pfp	42	17	15.4	1.6	1.2×10^{-18}
308pfp	45	19	12.5	6.5	1.4×10^{-19}
309pfp (gouge)	45	19	24.0	-5.0	unknown
310pfp	45	19	4.4	14.6	5.0×10^{-23}
311pfp	23	10	2.6	7.4	4.2×10^{-20}

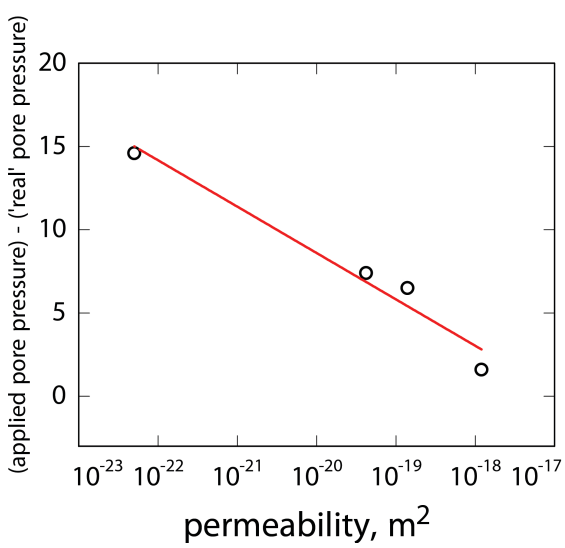

Figure 3 – Plot of permeability on a log scale vs. the difference between the applied and 'real' pore pressures.

As shown in Table 1, the applied pore pressure minus the real pore pressure appears to scale inversely with permeability. In the semi-log plot of Figure 3, we plot the difference between the applied fluid pressure and the estimate of the real fluid pressure vs. the permeability. As shown in the figure, there is a strong inverse correlation between the permeability of the various rocks and the difference between the applied and real pore pressures. The data indicate that the reduction in pore pressure due to dilatancy (and perhaps microcracking) is larger for samples of lower permeability, due to the difficulty of equilibrating the applied pore pressure with the pore pressure on the fault, since the applied pore pressure must communicate with the fault zone through the low permeability rock.

The role of dilatancy in fluid pressurization – Our experiments suggest that fault-normal dilation and compaction play a critical role in determining whether or not fluid pressurization effects are observed. In the bare-surface experiments, slow and then rapid sliding at the beginning of the experiments, over a remarkably consistent sliding displacement of ~0.5 m, led to a marked dilation of the fault zone. In Experiment 310pfp, on the lowest permeability sample (5×10^{-23} m^2), the dramatic influence of dilation, causing marked dilation hardening, is readily observable. After initial sliding at the very beginning of that experiment, sliding was stopped until pore fluid flowed into the sample and the friction at a resumed sliding rate of 1 μm/s was exactly the value expected (~0.8) for the nominal effective normal stress, i.e. the normal stress on the fault (45 MPa) minus the fluid pressure (19 MPa). However, as the sliding rate was increased above 1 μm/s, a huge increase in the apparent friction coefficient, up to 1.3, was observed, as shown in Figure 4. This may be attributed to the observed dilation and the resulting decrease in fluid pressure. Because this sample has such a low permeability, once the dilation occurs, it is difficult to fill the dilated fault zone with additional fluid, since the externally applied pressure must communicate with the fault zone through the impermeable rock. The fluid pressure therefore remains low and the friction coefficient therefore high due to dilatancy hardening. Dilatancy continues to at least 0.5 m of slip. Though dilation (and compaction) clearly must have modifying effects on thermal pressurization, fault-normal displacements are not generally accounted for in most theoretical treatments of thermal pressurization (e.g., [*Andrews*, 2002;

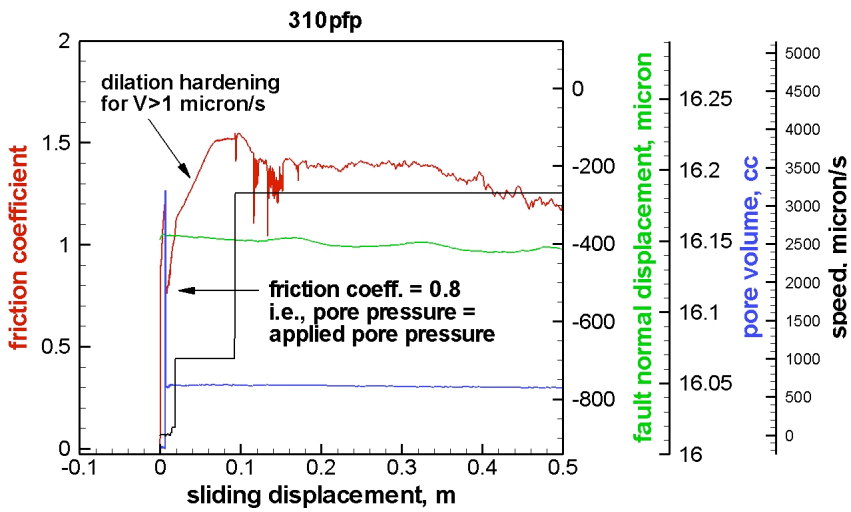

Figure 4 – Friction data at the very beginning of this test on our lowest permeability sample indicated that the pore fluid pressure was less than the applied fluid pressure. After a longer hold, friction decreased to 0.8 as expected based on the applied effective normal stress, i.e., the pore pressure reached the applied value. However, subsequent sliding caused enough dilatancy that the sample became strong and thermal pressurization never overcame the dilatancy.

Mase and Smith, 1985, 1987]). Note that although dilatancy is discussed by [*Rice*, 2006], he generally assumes that dilation causes an initial reduction of pore pressure over a small amount of slip; pore pressure reductions and dilatancy occurring for slip distances of 0.5 m or more have not been reported and are not treated in these theoretical analyses.

To further illustrate the strong influence of dilatancy on the fluid pressure of the experimental fault zones, we calculated the fluid pressure that would be required throughout Experiment 311pfp to yield a real friction coefficient of 0.8 (as observed in Experiments 297fd and 304tp1, for dry and saturated (drained) samples, respectively) given the applied normal stress and the observed values of friction. We then plotted the observed shear stresses, the calculated fluid pressures, and the fault-normal displacement vs. slip, as shown in Figure 5. As shown in the

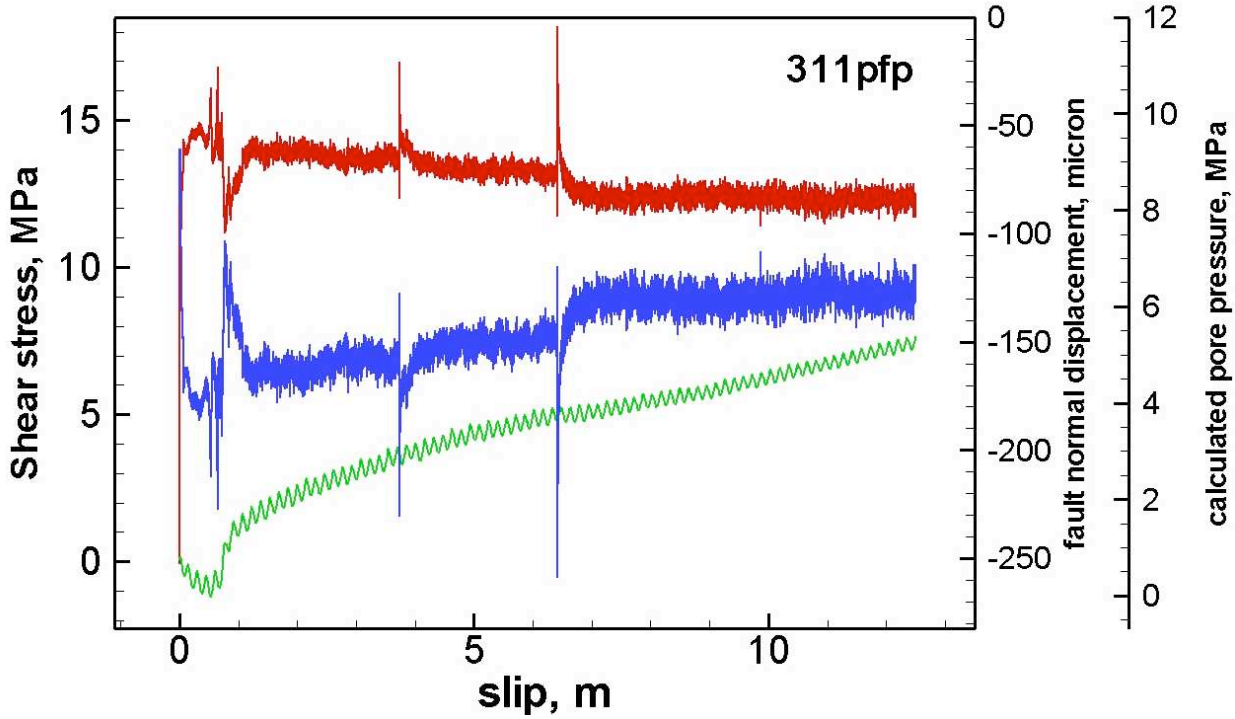

Figure 5 – Observed shear stress (red trace), associated (calculated) pore-fluid pressure (blue trace) required to obtain a friction coefficient of 0.8, and observed fault-normal displacement (green trace) for Experiment 311pfp. Spikes in observed shear stress and calculated pore pressure occur during long duration (> 12 hr) holds at a slip rate of V=0. Oscillations with amplitude of about 5 µm in the green curve have a wavelength of one revolution (155 mm) of the sample and are due to lack of perfect perpendicularity of the sample surfaces to the rotation axis.

Figure, at the beginning of the test, the calculated pore pressure (blue trace) is nearly 10 MPa, so it is equivalent to the applied fluid pressure of 10 MPa. With the initiation of slip, however, over the first 0.5 m of slip, the sample is observed to dilate by 15-20 µm. That dilation appears to correspond very well, in duration and in form, with the calculated pore pressure required to satisfy the observed shear stress. That dilation likely causes a decrease in fluid pressure, to ~4 MPa, and a corresponding increase in shear stress, due to an increase in the effective normal stress. As the sample begins to compact at ~0.6 m of slip, the pore pressure likely increases, causing a decrease in effective normal stress and a corresponding decrease in friction. One might anticipate that once enough compaction occurred to bring the fault-normal displacement value back to the value observed before the initial dilation, that the pore pressure would increase again. However, sliding to many meters of slip causes spallation and the development of crush zones along the inner and outer edges of the slip surfaces, and likely cracking on the fault surface, which increase the available pore space, requiring fluid replenishment from the external fluid reservoir, a very slow process for low-permeability samples. The long-term observed overall compaction trend may cause or contribute to the inferred trend of increasing fluid pressure, causing a corresponding decrease in the observed shear stress.

The results of our experiments suggest that to minimize the fluid-pressurization-limiting effects of dilation in future experiments, we will conduct experiments in the following manner 1) allow the samples to undergo enough sliding so that a trend of compaction is established, 2) set the sliding velocity to zero, 3) allow enough time for the pore pressure to return to its externally applied value, and 4) commence sliding at high velocity.

Observations of thermal pore-fluid pressurization? - Finally, we call attention to the possibility that pore-fluid pressurization appears to have occurred in Experiment 311pfp. In that experiment, as shown in Figure 5, the sample was slid initially at a sliding velocity of 3.2 mm/s for ~3.8 m of slip. At that point, the sliding velocity was set to zero and the sample sat stationary overnight. During that time, the fault zone initially compacted (not shown on the scale of Figure 5), then dilated due to fluid infiltration into the fault zone as the pore fluid pressure in the fault zone was equilibrating with the external pressure, as shown in Figure 6. The dilation continued but slowed dramatically, presumably as the fluid pressure got closer and closer to the applied value. At the step back to the high slip rate (3.2 mm/s) the sample dilates and the friction increases, presumably due to an increase in effective normal stress. This increase in friction is also convolved, however, with the increase in state at zero sliding velocity that accompanies any hold, and with the direct effect due to the step from V=0 to 3.2 mm/s. However, and most interestingly, over the next ~0.5 m of slip (see Figure 5), friction is observed to follow an exponential-like decreasing trend, at which point the friction levels off to a steady value. After sliding at 3.2 mm/s, the sample was again held stationary at V=0 and the fault was allowed to equilibrate again with the external pressure, yielding compaction data nearly identical to those in Figure 6. On stepping from V=0 to V=4.8 mm/s (see Figure 5), friction again increased sharply, due to the increase in state during the hold, the dilation that occurs at the velocity change (i.e., dilation hardening) and the friction direct effect. These exponential-like decays in friction are reminiscent of the decays shown in Figure 3 of Rice's thermal pressurization theory paper [*Rice*, 2006] although they do not have the multi-scale character that persists with displacement in that theoretical treatment.

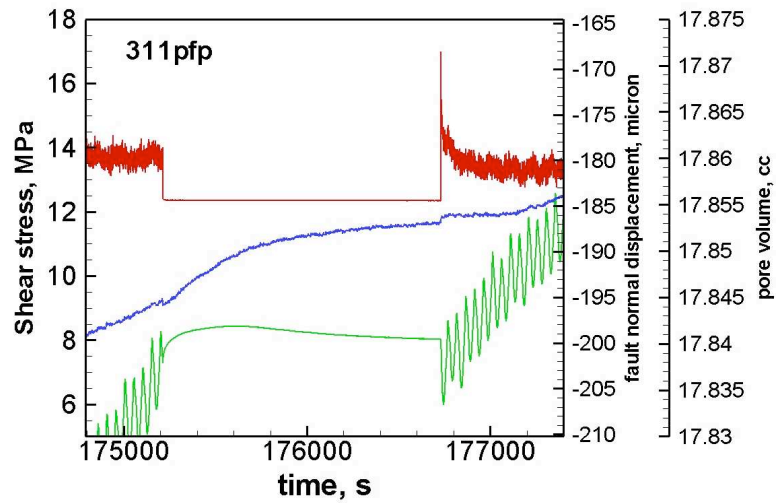

Figure 6 – Plot of shear stress (in red), fault normal displacement (in green), and pore volume (cm^3, in blue) for hold at 3.8 m of slip in Figure 5. Note the initial compaction, then dilation, as the fluid infiltrates the fault zone. The diminishing dilation and the decreasing rate of pore volume increase indicate that the fault zone is equilibrating with the externally applied fluid pressure.

To understand why we observe only this small amount of thermal pressurization weakening, while the theoretical predications of [*Mase and Smith*, 1985, 1987] and of [*Rice*, 2006] are of more dramatic and longer-lived weakening, we have analyzed the thermal histories in our samples and compared them with the expectations based on a fault in an infinite medium. The results of these calculations are shown in Figures 7 and 8 which contain both FEM computations as well as calculations based on the simple equations of [*Carslaw and Jaeger*, 1959].

As the lower-most curve in Figure 7 shows, the maximum temperature expected from the 3.2 mm/s sliding interval that begain at about 3.7 m of slip in experiment 311pfp is only about 45 °C. The temperature distribution after the 2.69 m of slip lasting 850 sec is shown in Figure 8a and 8b. These calculations suggest that the temperatures in our experiments thus far may be too

low to observe thermal pressurization behavior. In subsequent tests, the fault surface temperatures will be increased by conducting experiments at much higher normal stresses.

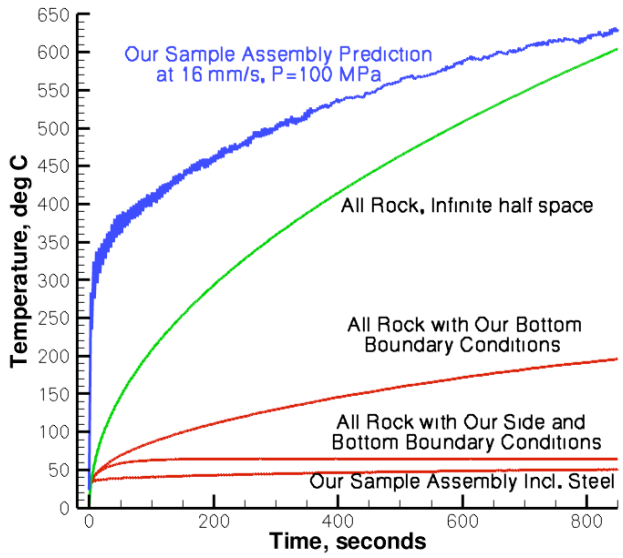

Figure 7 – Plots of temperature calculated on the fault surface for Run 311pfp for the 2.69 m of slip at 3.2 mm/s for 850 seconds at the observed shear strength of ~13.5 MPa (see the data from 311pfp between 3.7 and 5.4 m of slip in Figure 5). The red curves are calculated with a FEM whereas the green curve is an analytical solution. The blue curve shows the temperatures that are predicted to occur if in the future we slide at larger normal stresses and higher velocities. As is also shown in the FEM temperature maps of Fig. 8, the expected temperatures for a fault in an infinite medium cannot be attained in a sample assembly of finite size.

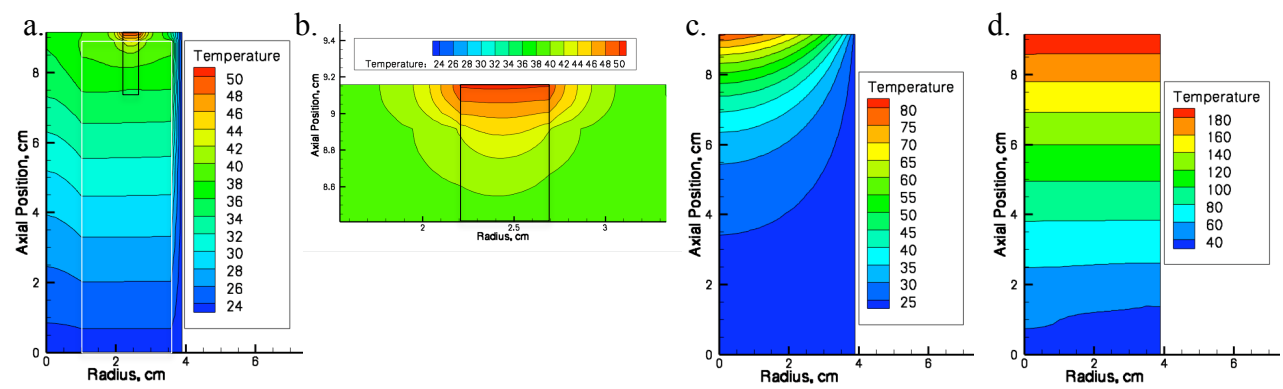

Figure 8 – Finite element models of the temperature distribution in our sample assembly after slip of 2.69 m at 3.2mm/s with the observed shear stress in Experiment 311pfp of 13.5 MPa. The assembly has axial symmetry with the axis at zero radius. The top of the drawing is a symmetry plane with the material above it imposing rotary shear on the illustrated region. Parts (a) and (b) are for our actual sample assembly that includes the rock sample, outlined with a black box, and steel, outlined with a white box in (a). Part (b) is a detail of the sample area from (a). Parts (c) and (d) show the effect of replacing all the rock and steel with rock and applying sliding with the same shear stress over the entire top of the sample. In (c) and (d) the bottom at an axial position of 0.0 has a boundary condition of 23 °C, and in (c) this temperature is also imposed at the outer radius of 3.81 cm. The effect of these boundary conditions is to limit the maximum temperature that can be attained as can be seen by comparison with the infinite medium plot in green in Fig. 7.

Looking Ahead

Our experimental results, and what we have learned about the procedures needed to understand both dilatancy and thermal pressurization, places us in an excellent position to conduct more definitive experiments in experiments to be conducted in the coming year. In particular, by sliding at up to 16 mm/s at a confining pressure of 100 MPa, our modeling suggests that the temperature rise should be up to 600 ^{o}C, rather than the ~25 ^{o}C rise estimated

for our current results. To minimize the fluid-pressurization-limiting effects of dilation, we believe that new experiments will prove to be useful in which 1) enough sliding is accrued that a trend of compaction is established, 2) the sliding velocity is then set to zero, 3) enough time is allowed for the pore pressure to return to its externally applied value, and 4) then sliding is commenced at high velocity. In these tests, we will look not only for changes in shear stress associated with thermal pressurization, but also changes in the previously established compaction trend. This procedure, in concert with thermal modeling and direct measurements of temperature very close to the sliding surface, should allow a conclusion to be reached concerning the operation of thermal pressurization in our experiments and in nature. In particular, we will determine the role that dilatancy may have in certain situations to diminish or eliminate thermal pressurization.

Geophysical implications

All of the weakening mechanisms we are studying have profound implications for the magnitude of stress drops during earthquakes and consequently for the magnitude of strong ground shaking. The manner in which fault strength varies with displacement and slip velocity, as well as the rate at which healing occurs as slip velocity decreases behind the rupture tip, can control the mode of rupture propagation, i.e., as a crack or as a self-healing slip pulse. Furthermore, these data can be important for resolving questions concerning stress levels in the crust. If coseismic friction is low, and the magnitudes of dynamic stress drops are constrained to modest values by seismic data, then the tectonic stress acting on faults must also be modest. We may have a strong crust that is nevertheless able to deform by faulting under modest tectonic stresses if the strength is overcome at earthquake nucleation sites by local stress concentrations and at other places along the fault by dynamic stress concentrations at the rupture front. Thus, understanding high-speed friction is important not only for practical matters related to predicting strong ground motions and resulting damage, but also for answering major scientific questions receiving considerable attention and funding, e.g., the strength of the San Andreas Fault / the Heat-Flow Paradox, the question that ultimately was responsible for the SAFOD project.

PUBLICATIONS RESULTING FROM THIS WORK

Goldsby, D. L., and T. E. Tullis (2011), Flash heating leads to low strength of crustal rocks at earthquake slip rates, Science, 334, 216-218, DOI: 210.1126/science.1207902.

REFERENCES CITED

Andrews, D. J. (2002), A fault constitutive relation accounting for thermal pressurization of pore fluid, J. Geophys. Res., 107, 12.

Beeler, N. M., T. E. Tullis, and D. L. Goldsby (2008), Constitutive relationships and physical basis of fault strength due to flash-heating, J. Geophys. Res., 113, B01401, doi:01410.01029/02007JB004988.

Bizzarri, A., and M. Cocco (2006a), A thermal pressurization model for the spontaneous dynamic rupture propagation on a three-dimensional fault: 2. Traction evolution and dynamic parameters, J. Geophys. Res., 111, B05304, doi:05310.01029/02005JB003864.

Bizzarri, A., and M. Cocco (2006b), A thermal pressurization model for the spontaneous dynamic rupture propagation on a three-dimensional fault: 1. Methodological approach, J. Geophys. Res., 111, B05303, doi:05310.01029/02005JB003862.

Carslaw, H. S., and J. C. Jaeger (1959), Conduction of Heat in Solids, 510 pp., Claredon Press, Oxford.
Di Toro, G., D. L. Goldsby, and T. E. Tullis (2004), Friction falls toward zero in quartz rock as slip velocity approaches seismic rates, Nature, 427, 436-439.
Fredrich, J. T., and T.-f. Wong (1986), Micromechanics of thermally induced cracking in three crustal rocks, J. Geophys. Res., 91, 12,743-712,764.
Goldsby, D. L., and T. E. Tullis (2002), Low frictional strength of quartz rocks at subseismic slip rates, Geophys. Res. Lett., 29(17), 1844, doi:1810.1029/2002GL015240.
Goldsby, D. L., and T. E. Tullis (2011), Flash heating leads to low strength of crustal rocks at earthquake slip rates, Science, 334, 216-218, DOI: 210.1126/science.1207902.
Kohli, A. H., D. L. Goldsby, G. Hirth, and T. E. Tullis (2011), Flash weakening of serpentinite at near-seismic slip rates, J. Geophys. Res., 116, B03202, doi:10.1029/2010JB007833.
Lachenbruch, A. H. (1980), Frictional heating, fluid pressure, and the resistance to fault motion, J. Geophys. Res., 85, 6249-6272.
Lapusta, N., and J. R. Rice (2004a), Earthquake sequences on rate and state faults with strong dynamic weakening, Eos. Trans. Am. Geophys. Union, Fall Meeting Suppl., 85(47), T22A-05.
Lapusta, N., and J. R. Rice (2004b), Earthquake sequences on rate and state faults with strong dynamic weakening, paper presented at 2004 SCEC Annual Meeting Proceedings and Abstracts, Southern California Earthquake Center, PalmSprings, California, 2004.
Lee, T. C., and P. T. Delaney (1987), Frictional Heating and Pore Pressure Rise Due to a Fault Slip, Geophysical Journal of the Royal Astronomical Society, 88(3), 569-591.
Mase, C. W., and L. Smith (1985), Pore-fluid pressures and frictional heating on a fault surface, Pure Appl. Geophys., 122, 583-607.
Mase, C. W., and L. Smith (1987), Effects of frictional heating on the thermal hydrologic and mechanical response of a fault, J. Geophys. Res., 92, 6249-6272.
Noda, H. (2008), Frictional constitutive law at intermediate slip rates accounting for flash heating and thermally activated slip process, J. Geophys. Res., doi:10.1029/2007JB005406.
Noda, H., and T. Shimamoto (2005), Thermal pressurization and slip-weakening distance of a fault: An example of the Hanaore fault, southwest Japan, Bull. Seis. Soc. Am., 95(4), 1224-1233.
Noda, H., and N. Lapusta (2010), Three-dimensional earthquake sequence simulations with evolving temperature
and pore pressure due to shear heating: Effect of heterogeneous hydraulic diffusivity, J. Geophys. Res., 115, B12314.
Noda, H., E. M. Dunham, and J. R. Rice (2009), Earthquake ruptures with thermal weakening and the operation of major faults at low overall stress levels, J. Geophys. Res., 114 (B07302), doi:10.1029/2008JB006143.
Rempel, A. W., and J. R. Rice (2006), Thermal pressurization and onset of melting in fault zones, Journal of Geophysical Research-Solid Earth, 111(B9), B09314, doi:09310.01029/02006JB004314.
Rice, J. R. (2006), Heating and weakening of faults during earthquake slip, Journal of Geophysical Research-Solid Earth, 111(B5), doi:10.1029/2005JB004006.
Rice, J. R., and M. Cocco (2007), Seismic fault rheology and earthquake dynamics, in The Dynamics of Fault Zones, edited by M. R. Handy, p. in press, MIT Press, Cambridge, Mass.
Rice, J. R., E. M. Dunham, and H. Noda (2010), Thermo- and hydro-mechanical processes along faults during rapid slip, in Meso-Scale Shear Physics in Earthquake and Landslide Mechanics, edited by Y. Hatzor, J. Sulem and I. Vardoulakis, pp. 3-16, CRC Press.

Roig Silva, C., D. L. Goldsby, G. Di Toro, and T. E. Tullis (2004a), The role of silica content in dynamic fault weakening due to gel lubrication, paper presented at 2004 SCEC Annual Meeting Proceedings and Abstracts, Southern California Earthquake Center, Palm Springs, California.

Roig Silva, C., D. L. Goldsby, G. Di Toro, and T. E. Tullis (2004b), The role of silica content in dynamic fault weakening due to gel lubrication, Eos. Trans. Am. Geophys. Union, Fall Meeting Suppl., 85(47), T21D-07.

Schmitt, S. V., and P. Segall (2009), Thermal pressurization during “slip law” frictional earthquake nucleation, Poster, 2009 SCEC Annual Meeting.

Segall, P., and J. R. Rice (2006), Does shear heating of pore fluid contribute to earthquake nucleation?, Journal of Geophysical Research-Solid Earth, 111 (B09316), doi:10.1029/2005JB004129.

Sibson, R. H. (1973), Interactions between temperature and fluid pressure during earthquake faulting - A mechanism for partial or total stress relief, Nature, 243, 66-68.